ACS APPLIED MATERIALS & INTERFACES

Research Article

www.acsami.org

Synergistic Bifunctional Catalyst Design based on Perovskite Oxide Nanoparticles and Intertwined Carbon Nanotubes for Rechargeable Zinc–Air Battery Applications

Dong Un Lee, Hey Woong Park, Moon Gyu Park, Vugar Ismayilov, and Zhongwei Chen*

Department of Chemical Engineering Waterloo Institute for Nanotechnology Waterloo Institute for Sustainable Energy, University of Waterloo, Waterloo, ON Canada, N2L 3G1

Supporting Information

ABSTRACT: Advanced morphology of intertwined core–corona structured bifunctional catalyst (IT-CCBC) is introduced where perovskite lanthanum nickel oxide nanoparticles ($LaNiO_3$ NP) are encapsulated by high surface area network of nitrogen-doped carbon nanotubes (NCNT) to produce highly active and durable bifunctional catalyst for rechargeable metal–air battery applications. The unique composite morphology of IT-CCBC not only enhances the charge transport property by providing rapid electron-conduction pathway but also facilitates in diffusion of hydroxyl and oxygen reactants through the highly porous framework. Confirmed by electrochemical half-cell testing, IT-CCBC in fact exhibits very strong synergy between $LaNiO_3$ NP and NCNT demonstrating bifunctionality with significantly improved catalytic activities of oxygen reduction reaction (ORR) and oxygen evolution reaction (OER). Furthermore, when compared to the state-of-art catalysts, IT-CCBC outperforms Pt/C and Ir/C in terms of ORR and OER, respectively, and shows improved electrochemical stability compared to them after cycle degradation testing. The practicality of the catalyst is corroborated by testing in a realistic rechargeable zinc–air battery utilizing atmospheric air in ambient conditions, where IT-CCBC demonstrates superior charge and discharge voltages and long-term cycle stability with virtually no battery voltage fading. These improved electrochemical properties of the catalyst are attributed to the nanosized dimensions of $LaNiO_3$ NP controlled by simple hydrothermal technique, which enables prolific growth of and encapsulation by highly porous NCNT network. The excellent electrochemical results presented in this study highlight IT-CCBC as highly efficient and commercially viable bifunctional catalyst for rechargeable metal–air battery applications.

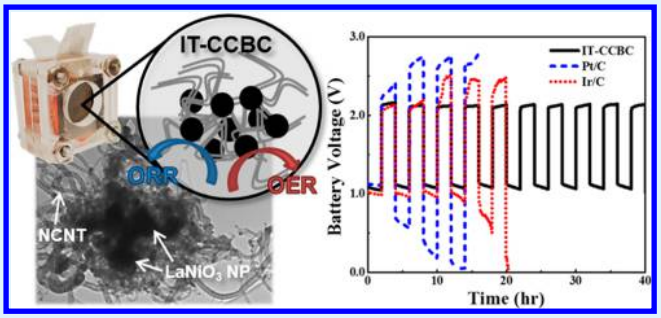

KEYWORDS: *lanthanum nickel oxide, perovskite, nitrogen doped carbon nanotubes, core–corona, bifunctional, oxygen reduction reaction, oxygen evolution reaction, metal–air battery*

INTRODUCTION

The nonrenewable natural sources of energy eventually face depletion due to limited reserves and our continued dependence on them.[1] In addition, the burning of fossil fuels increases the carbon dioxide emissions, which leads to severe global environmental concerns. To address the issues associated with heavily dependent usage of the natural energy sources, recent efforts in research have been focused on the development of alternative energy sources. One particular area of highly interesting and promising research is the investigation of reversible electrochemical energy conversion systems such as rechargeable battery technologies. To date, lithium-ion batteries are considered to be the most developed rechargeable battery system, demonstrating excellent Coulombic efficiency and cycle stability. However, relatively low energy density of lithium-ion batteries is one critical shortcoming of the technology, which makes it difficult to fulfill the ultimate requirements of highly energy-intensive applications such as electric vehicles (EV).[2−4] Alternatively, metal–air batteries such as zinc–air and lithium–air batteries are considered as one of the most promising rechargeable energy conversion and storage systems due to their extremely high theoretical energy densities.[4] In particular, zinc–air batteries, which consist of nonflammable and nonexplosive materials, are very attractive for applications such as EVs where safe operation is the top priority.[5−7] In addition, the high energy density of metal–air batteries can significantly extend the "drivable" range of the current lithium-ion based EVs. In spite of these promising features, metal–air batteries face some technical challenges, which must be addressed to make them commercially viable as the next generation energy system.[4,5,8] For instance, the operation of rechargeable metal–air batteries is dependent on the oxygen reduction reaction (ORR) and the oxygen evolution reaction (OER), which correspond to discharge and charge processes,

Received: October 27, 2014
Accepted: December 15, 2014
Published: December 15, 2014

DOI: 10.1021/am507470f
ACS Appl. Mater. Interfaces 2015, 7, 902–910

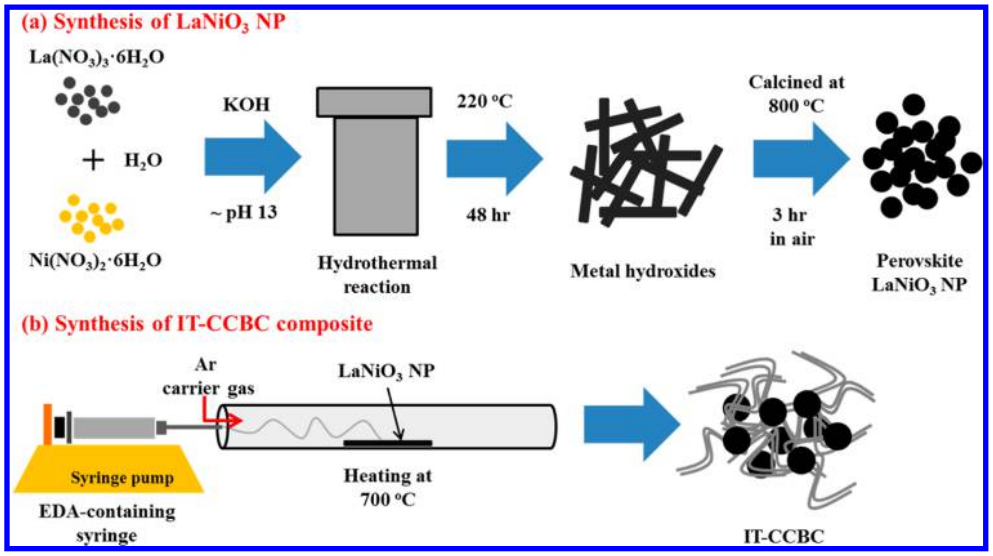

Figure 1. Schematic illustrations of (a) hydrothermal synthesis of $LaNiO_3$ NP and (b) injection CVD preparation of IT-CCBC.

respectively.[9,10] However, high overpotentials are associated ORR and OER due to the sluggish reaction kinetics, which lowers energy efficiency, thereby limiting the use of current metal−air batteries. The metal−air battery systems then require electrocatalysts in the air electrode to efficiently expedite the kinetics of the oxygen reactions to progress them at commercially practical rates.

Currently, precious metal-based catalysts such as platinum and iridium supported on carbon are known to be the most efficient at catalyzing the oxygen electrochemical reactions.[11−14] However, they are not only too costly for applications in a wide range of commercial products but also exhibit limited rechargeability due to various degradation mechanisms such as particle agglomeration, detachment, and poisoning.[15] To address these challenges, affordable and highly durable bifunctional catalysts have been developed to improve the charge/discharge performance and lifetime of metal−air batteries. For example, nonprecious transition metal oxides and their composites with graphitic carbon materials have been extensively demonstrated in the literature to show excellent catalytic activities.[3,16−18] Perovskite oxides, in particular, are known to be very promising for efficient bifunctional oxygen electrocatalysis due to their good cation ordering, which enhances the mobility of oxygen ions for improved catalytic activity.[19−21] In addition to the composition and crystal structure, morphology can also be tailored to further improve the catalyst electrochemical activity. One effective approach is to reduce the physical dimensions of the catalyst to obtain high surface area nanostructures with increased number of active sites, and another is to combine with high surface area carbon materials to enhance the electrically conductive pathway during the electrochemical reaction.

In this work, we introduce a composite consisting of lanthanum nickel oxide nanoparticles ($LaNiO_3$ NP) and nitrogen-doped carbon nanotubes (NCNT) as highly active and durable bifunctional catalyst for rechargeable zinc−air batteries. This composite has a unique morphology where $LaNiO_3$ NP are encapsulated by highly porous and intertwined network of NCNT resulting in a core−corona structure. The catalyst is bifunctionally active toward both ORR and OER and demonstrates synergy between the two components resulting in superior overall performance. The OER activity of the composite mainly stems from the size-controlled perovskite $LaNiO_3$ NP prepared by a simple hydrothermal method, while the ORR activity arises from NCNT grown by injection chemical vapor deposition (CVD). The unique composite morphology is a result of prolific growth of intertwined NCNT knitting the clusters of $LaNiO_3$ NP, creating an intimate contact between the two components to create a highly active electrocatalyst with enhanced electrochemical durability and synergistic effect. In fact, our previously reported composite created without morphological control resulted in a nonuniform NCNT growth over irregular surfaces of macrosized $LaNiO_3$ particles with significantly less interparticle interaction and limited electrocatalytic activity.[15] In contrast, current study presents highly tailored composite structure with nanosized perovskite nanoparticles to promote much favorable NCNT growth directly on and around $LaNiO_3$ NP. The electrochemical enhancements for the oxygen reactions obtained by the composite catalyst is thus due to carefully engineered morphology, which results in improved diffusion of reactants and charge transfer of active species through the intimate interparticle interactions of $LaNiO_3$ NP and NCNT.

EXPERIMENTAL SECTION

As illustrated in Figure 1a, perovskite $LaNiO_3$ NP were synthesized by simple hydrothermal technique. First, 1.0 mM of lanthanum nitrate hexahydrate ($La(NO_3)_3·6H_2O$, Aldrich) and 1.0 mM nickel nitrate hexahydrate ($Ni(NO_3)_2·6H_2O$, Aldrich) were dissolved in 35 mL of distilled deionized (DDI) water. The pH of the solution was adjusted to 13 by adding 6.0 M potassium hydroxide (KOH, Aldrich). Then, the solution was transferred to a Teflon-lined container of an autoclave. The autoclave was placed in a preheated oven at 220 °C and left at rest for 48 h. The resulting product from the autoclave was washed with DDI water and ethanol and collected by filtration followed by drying at 60 °C overnight. The product was ground and calcined in air at 800 °C for 3 h. Finally, the heat-treated product was ground again to obtain $LaNiO_3$ NP.

Next, as illustrated in Figure 1b, IT-CCBC was prepared by growing NCNT on $LaNiO_3$ NP via injection CVD. First, 20 mg of $LaNiO_3$ NP was dispersed in the solution of 0.5 wt % ferrocene ($C_{10}H_{10}Fe$, Aldrich) in ethanol by sonication. Then, the mixture was cast on the inside wall of a small quartz tube (18 mm O.D., 100 mm length), which was placed inside a horizontal tube furnace. As NCNT injection precursor solution, 2.5 wt % ferrocene in ethylenediamine (EDA) ($C_2H_8N_2$, Aldrich) was prepared, and 2 mL of it was loaded into a

DOI: 10.1021/am507470f
ACS Appl. Mater. Interfaces 2015, 7, 902−910

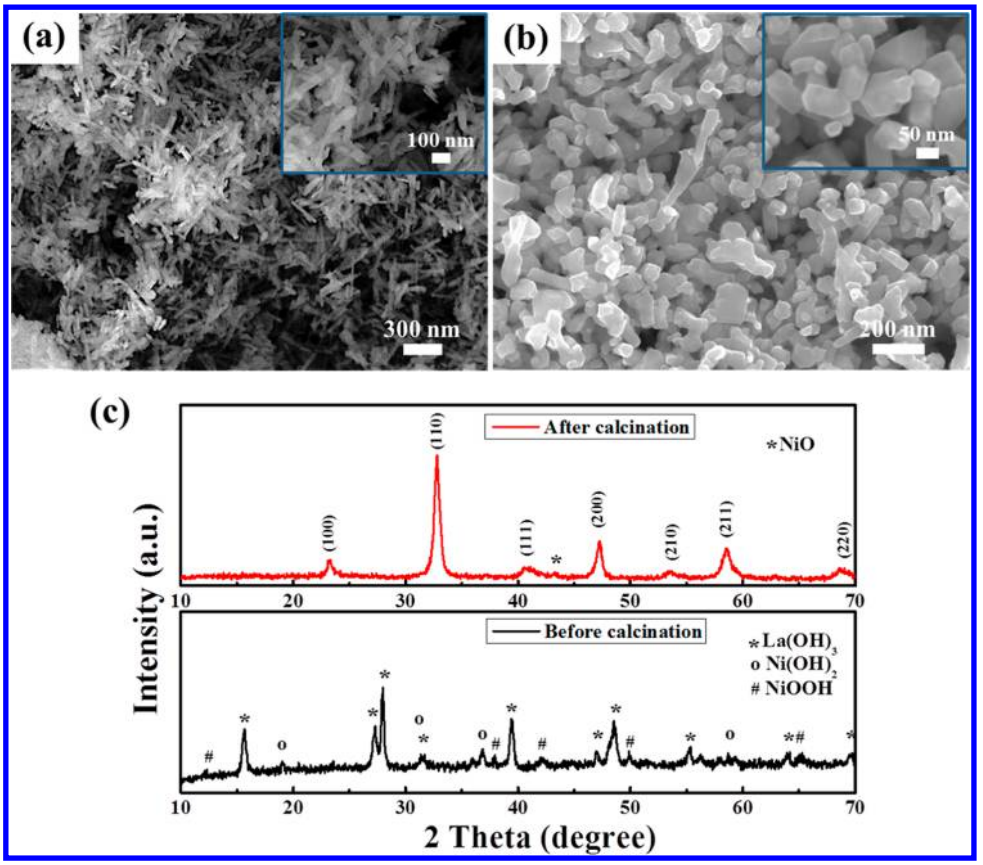

Figure 2. SEM images of $LaNiO_3$ NP (a) before and (b) after calcination. (insets) Magnified images. (c) XRD patterns of $LaNiO_3$ NP before and after calcination.

syringe. The precursor solution was then injected into the horizontal tube furnace with the discharge rate of 0.05 mL min^{-1} at 700 °C in Ar flow of 100 sccm. After injection, the furnace was cooled to room temperature, and IT-CCBC was collected as the final product.

For chemical and physical characterizations of IT-CCBC, the following methods were used in the study. Scanning electron microscopy (SEM) (LEO FESEM 1530) and transmission electron microscopy (TEM) (JEOL 2010F) were employed to observe the morphology and structure of $LaNiO_3$ NP, NCNT, and IT-CCBC. X-ray diffraction (XRD) (Brunker AXS D8 Advance) and X-ray photoelectron spectroscopy (XPS) (Thermal Scientific K-Alpha XPS spectrometer) were conducted to characterize crystalline phase and size of $LaNiO_3$ NP and to analyze the atomic composition of the elements in IT-CCBC, respectively. N_2 adsorption−desorption isotherms were obtained by Brunauer−Emmett−Teller (BET) method (Folio Micromeritics ASAP2020) to determine active surface area, pore volume, and size distribution of $LaNiO_3$ NP, NCNT, and IT-CCBC.

The electrocatalytic activity and durability of IT-CCBC were evaluated by rotating disc electrode (RDE) voltammetry using a potentiostat (CH Instrument 760D) and a rotation speed controller (Pine Instrument Co., AFMSRCE). The catalyst ink was prepared with a concentration of 4 mg mL^{-1} in ethanol-diluted Nafion solution and coated onto a glassy carbon disk electrode (5 mm OD) with IT-CCBC loading of 1.22 mg cm^{-2} as the working electrode. As comparisons, $LaNiO_3$ NP (mixed with Vulcan Carbon in 3:7 mass ratio), NCNT, 20 wt % platinum on carbon (Pt/C), and 20 wt % iridium on carbon (Ir/C) catalysts were prepared as working electrodes using the same process as that for IT-CCBC. As counter and reference electrodes, a platinum wire and saturated calomel electrode (SCE) were used, respectively, and 0.1 M KOH was used as the electrolyte. For the examination of the ORR activity, linear sweep voltammetry (LSV) was conducted using RDE at a scan rate of 10 mV s^{-1} in O_2-saturated electrolyte. Cyclic voltammetry (CV) was used to investigate the OER activity and durability in N_2-saturated electrolyte at a scan rate of 50 mV s^{-1}. The measured currents for ORR and OER were normalized by the area of the glassy carbon disk electrode, and the potentials were converted to reversible hydrogen electrode (RHE).

For the investigation of performance of IT-CCBC in a realistic metal−air battery, in-house designed zinc−air battery was prepared and tested using a multichannel potentiostat (Princeton Applied Research, VersaSTAT MC). A polished zinc plate as an anode, catalyst-coated gas diffusion layer (GDL) (Ion Power Inc., SGL Carbon 10 BB, 2.5 cm by 2.5 cm) as a cathode, and microporous membrane (25 μm polypropylene membrane, Celgard 5550) as a separator were used. 6.0 M KOH was used as the electrolyte. The catalyst layer coated on the GDL was prepared as follows. First, 9.4 mg of catalyst was dispersed in 1 mL of isopropanol and sonicated for 30 min, followed by addition of 67 μL of 5 wt % Nafion solution (LIQUion solution, Ion Power Inc.) to prepare a catalyst ink. The catalyst ink was then sprayed onto the GDL with a conventional airbrush. After spraying, the GDL was dried at 60 °C for 1 h. The catalyst loading was determined by the difference in the weight of the GDL before and after spraying. The actual area with loading of ca. 0.78 mg cm^{-2} of the cathode exposed to the electrolyte and air was 2.84 cm^2. As controls, commercial 20 wt % Pt/C and Ir/C catalysts with the same loading were prepared using the same method as IT-CCBC.

For rechargeable single-cell zinc−air battery testing, the charge and discharge profiles were obtained by the galvanodynamic method scaling the current from 0 to 200 mA at a rate of 5 mA s^{-1}. The pulse charge/discharge (C/D) cycling was tested by the recurrent galvanic pulse method using an applied current of 50 mA with each cycle consisting of 5 min of discharge followed by 5 min of charge. The extended cycling was conducted similar to the pulse C/D but with each cycle consisting of 2 h of discharge followed by 2 h of charge. Electrochemical impedance spectroscopy (EIS) was conducted by operating the battery at constant cell potential of 0.8 V and alternating

DOI: 10.1021/am507470f
ACS Appl. Mater. Interfaces 2015, 7, 902−910

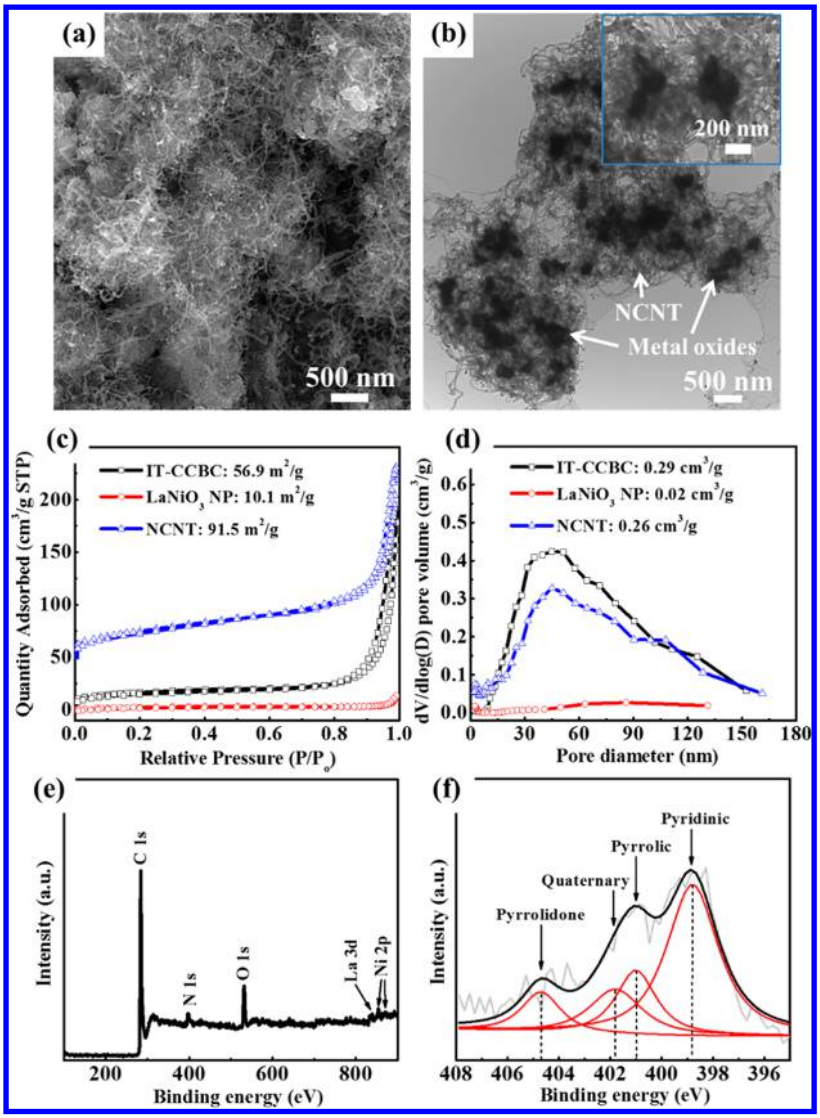

Figure 3. (a) SEM and (b) TEM images of IT-CCBC. (inset) Magnified image of the composite. (c) N_2 adsorption−desorption isotherms obtained at 77 K. (d) Pore size distribution obtained by BJH method of IT-CCBC, $LaNiO_3$ NP, and NCNT. (e) Full XPS spectrum of IT-CCBC. (f) Deconvoluted high-resolution N 1s XPS spectrum of IT-CCBC.

current (AC) amplitude of 20 mV with its frequency ranging from 100 kHz to 0.1 Hz.

RESULTS AND DISCUSSION

The morphology and crystal phase of $LaNiO_3$ NP after the hydrothermal synthesis were investigated by SEM and XRD analyses. Nanostructures with characteristic rodlike morphology are revealed by SEM, as shown in Figure 2a, and are confirmed by XRD to be composed of $La(OH)_2$, $Ni(OH)_2$, and NiOOH metal hydroxide species as shown in Figure 2c, consistent with results reported in the literature.[22−24] After calcination in air at 800 °C, nanorods are slightly increased in size ranging from 100 to 200 nm as shown in Figure 2b, however, still maintaining its nanoscale dimensions for enhanced surface area. The particle size expansion is most likely due to the agglomeration during the calcination carried out at an elevated temperature. The conversion of the nanostructures from metal hydroxide species into perovskite phase $LaNiO_3$ with a trace amount of NiO after calcination is confirmed by XRD, consistent with previously published results.[15] The injection CVD technique is then used to grow NCNT directly onto $LaNiO_3$ NP. Prolific growth and excellent coverage of NCNT encapsulating $LaNiO_3$ NP within its highly porous and intertwined network is revealed by SEM as shown in Figure 3a. The thermal gravimetric analysis (Supporting Information, Figure S2) revealed that IT-CCBC actually consists of 72% NCNT, which is significantly higher than that of our previously reported $LaNiO_3$/NCNT composite (64.2%).[15] This significant increase in the amount of NCNT is in accordance with the idea that high surface area nanosized metal oxide particles promote much favorable growth of NCNT by providing more growth sites. The morphology of IT-CCBC is further characterized by TEM as shown in Figure 3b, which clearly shows $LaNiO_3$ NP clusters completely encapsulated by the network of NCNT. As a comparison, NCNT is grown without the presence of $LaNiO_3$ NP, which clearly shows a typical bamboolike tubular structure (Supporting Information, Figure S1).[25] Next, the BET analysis was conducted to obtain N_2 adsorption−desorption isotherms as shown in Figure 3c, where IT-CCBC shows significantly higher surface area of 56.9 $m^2\ g^{-1}$ compared to $LaNiO_3$ NP due to excellent coverage of the nanoparticles by high surface area

DOI: 10.1021/am507470f
ACS Appl. Mater. Interfaces 2015, 7, 902−910

NCNT. Furthermore, the Barrett–Joyner–Halenda (BJH) method revealed the pore volume of IT-CCBC to be the largest, as shown in Figure 3d, which is likely due to the unique composite morphology created by the encapsulation of nanoparticle clusters by intertwined NCNT network resulting in a highly porous structure. The elemental composition of IT-CCBC is analyzed by XPS as shown in Figure 3e, where peaks that correspond to $LaNiO_3$ and NCNT are clearly observed. The main peak of C 1s located at 284.1 eV is attributed to the sp^2 configuration of the conjugated graphitic carbon making up the walls of NCNT.[26] Furthermore, a strong N 1s peak found at 398.1 eV confirms successful incorporation of nitrogen species in NCNT. The peaks that correspond to $LaNiO_3$ NP (i.e., La 3d and Ni 2p) show relatively lower intensities, which is most likely due to very well-covered metal oxide nanoparticles by the NCNT network as consistently observed in the above SEM and TEM images. The N 1s peak is deconvoluted as shown in Figure 3f to further elucidate the existence of various nitrogen species in NCNT. Among the four nitrogen species found (pyridinic, pyrrolic, quaternary, and pyrrolidone), pyridinic and pyrrolic nitrogen configurations in NCNT are known to contribute to the ORR activity, which is very attractive for combining with OER active perovskite metal oxide to create highly efficient bifunctional catalysts.[27−30]

The half-cell testing is conducted to evaluate the electrochemical bifunctional activity of IT-CCBC toward both ORR and OER. The measured ORR currents were corrected by subtracting the background current obtained by carrying out the same measurement in a N_2-saturated electrolyte. The ORR polarization curves resulting from the cathodic linear sweep voltammetry at the rotation rate of 900 rpm is shown in Figure 4a. The ORR currents of IT-CCBC show significant improvements over $LaNiO_3$ NP in terms of onset, half-wave potentials, and limiting current density. These enhancements in the ORR activity are attributed to the addition of NCNT with heterogeneous nitrogen species, which creates catalytic ORR active sites.[10,25,31] In addition, the fact that IT-CCBC exhibits half-wave potential superior even to that of NCNT is a clear indication that the synergistic effect is obtained by combining $LaNiO_3$ NP with NCNT. The excellent activity is likely attributed to the improved charge transport by the composite and faster diffusion of active species due to the high surface area, both of which in turn enhance the ORR kinetics. The degree of the ORR activity of IT-CCBC in terms of the number of electrons transferred during the reaction is analyzed by using Koutechý–Levich (K–L) plot obtained with the RDE measurements at various rotation speeds (Supporting Information, Figure S3a). The linear fitting of i^{-1} versus $\omega^{-0.5}$ K–L plot allows the determination of the number of electrons (n) involved during the ORR,[32,33] where n is found to be 4.0, 3.9, and 4.0 at selected potentials of 0.70, 0.60, and 0.50 V (vs RHE), respectively (Supporting Information, Figure S3b). This is indicative of the ORR occurring with a swift kinetics by the pseudo four-electron reduction pathway (i.e., $O_2 + 2H_2O + 4e^- \rightarrow 4OH^-$), instead of the two-electron reaction, which produces undesirable oxygen species. While ORR governs the discharge process of a metal–air battery, OER is responsible for the charge process, which is critical for rechargeable applications. The enhanced OER catalytic activity of IT-CCBC is observed by superior OER currents compared to those of $LaNiO_3$ NP and NCNT as shown in Figure 4b. Between the potential range of 1.2 and 1.6 V (vs RHE), the relatively low current peaks are ascribed to the characteristic

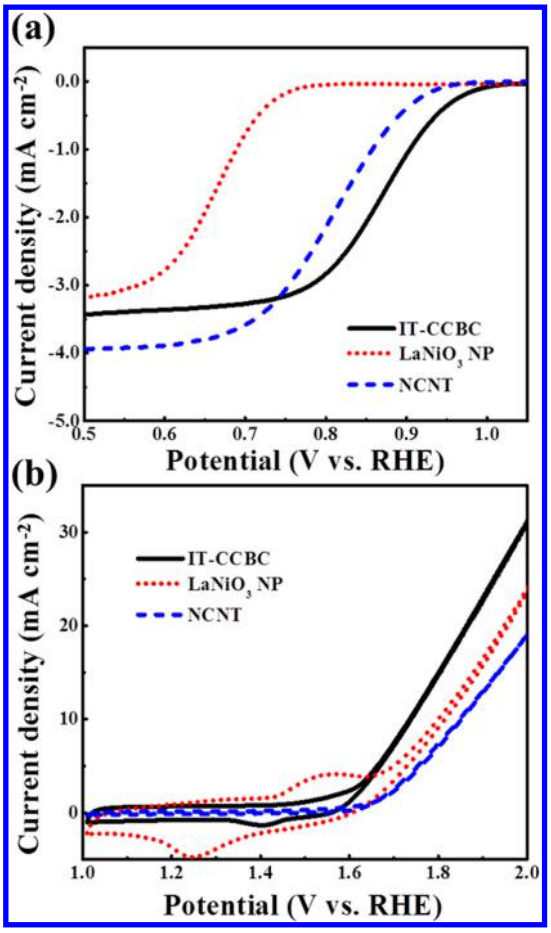

Figure 4. (a) ORR and (b) OER polarization curves obtained at rotation speed of 900 rpm with 10 mV s^{-1} and 50 mV s^{-1} scan rates, respectively, of IT-CCBC, $LaNiO_3$ NP, and NCNT.

electrochemical reactions of Ni,[15] while the current generated after 1.6 V is due to the OER. Similar to ORR, IT-CCBC is observed to exhibit synergy toward OER, clearly evident from the highest current obtained at 2.0 V compared to both $LaNiO_3$ NP and NCNT. The significant improvement in OER is also attributed to the facilitated charge transfer by the conductive pathway created by the NCNT network, as well as the highly porous morphology of IT-CCBC enabling better diffusion of active species such as the evolved O_2 during the electrochemical reaction. The catalytic activity of IT-CCBC as a practically viable catalyst is demonstrated by its comparable half-wave potential and current density to those of commercial state-of-art Pt/C catalyst as shown in Figure 5a. In terms of OER activity, however, the commercial state-of-art Ir/C catalyst is slightly better performing than IT-CCBC in terms of onset potential and OER current density as shown in Figure 5b. The merit of IT-CCBC is compensated by significantly lower price of nonprecious elements used to produce the catalyst, in addition to the fact that IT-CCBC is bifunctionally active toward both ORR and OER, whereas the precious Pt/C and Ir/C catalysts are not only very expensive but also only unifunctionally active toward either ORR (Pt/C) or OER (Ir/C). The cost effectiveness and synergistically bifunctional activity of IT-CCBC is further highlighted by its electrochemical durability, which makes it highly suited for implementations in commercial rechargeable metal–air batteries. The electrochemical durability of the catalyst is

DOI: 10.1021/am507470f
ACS Appl. Mater. Interfaces 2015, 7, 902–910

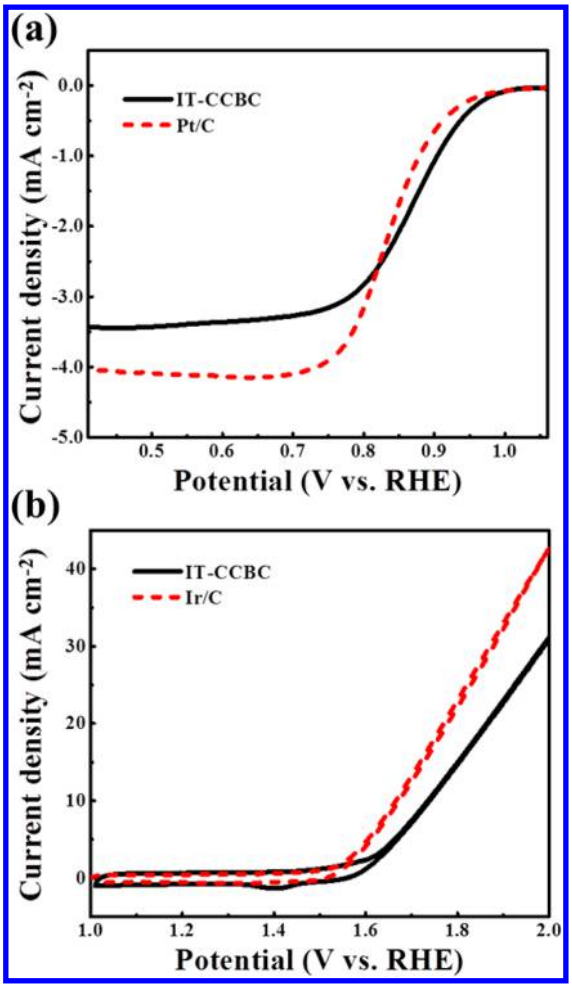

Figure 5. (a) ORR polarization curves of IT-CCBC and Pt/C and (b) OER polarization curves of IT-CCBC and Ir/C obtained at rotation speed of 900 rpm.

investigated by analyzing the entire working range of a rechargeable metal–air battery, where a wide potential window of 0.0 to 2.0 V was used to obtain CV curves before and after full-range degradation testing (FDT). IT-CCBC demonstrates excellent cycle stability as observed in Figure 6a by negligible current density fading before and after cycling, retaining most of its OER activity even after 500 cycles. On the other hand, Pt/C exhibits only 200 cycles before the measured current drops significantly, as shown in Figure 6b, due to its poor electrochemical stability. The limited electrochemical durability of Pt/C is likely due to the corrosion of the carbon support, as well as platinum dissolution, and separation from the support then agglomeration during the OER occurring at the higher potential regime.[15] For these reasons, the current density resulting from Pt/C is likely a mix of the OER current, and the current generated by various degradation mechanisms. Ir/C demonstrates less severe current density fading compared to Pt/C, as shown in Figure 6c, but still resulted in significant performance drop even after 200 cycles. The full-range cycle stability testing thus confirms excellent durability of IT-CCBC, which is attributed to the unique morphology of $LaNiO_3$ NP clusters and NCNT strongly coupled by the intertwined network.

The catalytic performance of IT-CCBC as bifunctional electrocatalyst is further highlighted by testing in a rechargeable

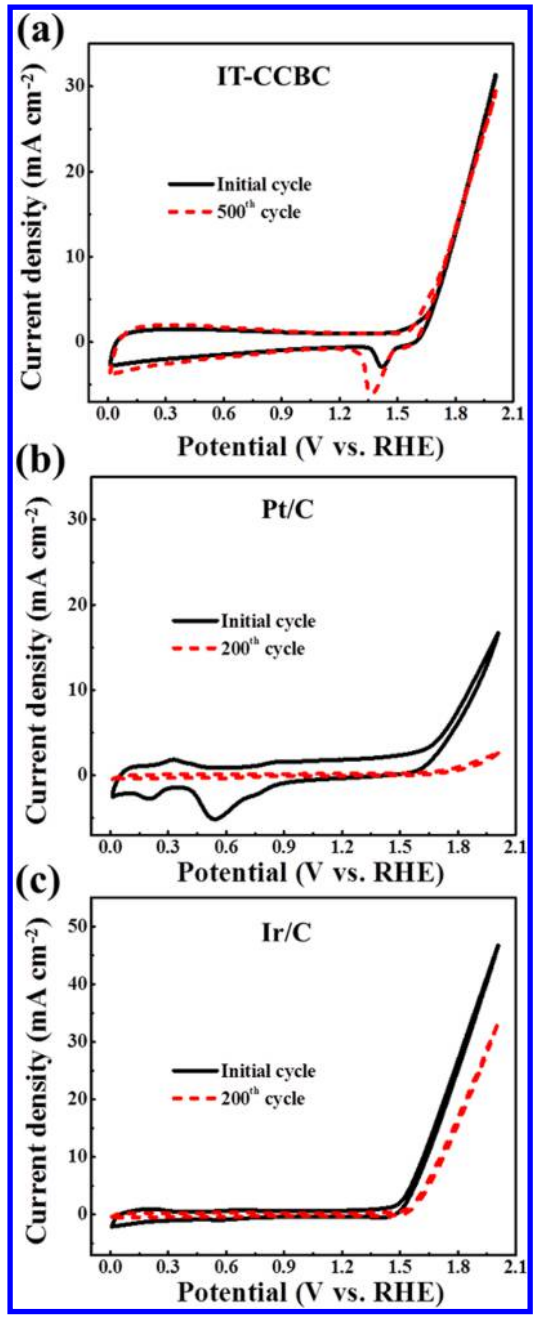

Figure 6. Cyclic voltammograms obtained before and after FDT of (a) IT-CCBC, (b) Pt/C, and (c) Ir/C obtained at rotation speed of 900 rpm in N_2-saturated electrolyte.

single-cell zinc–air battery prototype (Supporting Information, Figure S4). The battery is operated in ambient condition using atmospheric air, unlike other research groups that use purged oxygen as the source of fuel to demonstrate realistic and practical operation. A zinc plate and catalyst-coated GDL are employed as anode and air cathode, respectively, and 6.0 M KOH is used as electrolyte based on our previous report.[29] Figure 7a shows the galvanodynamic behaviors of IT-CCBC, Pt/C, and Ir/C during both battery charge and discharge. During discharge, the polarization behavior of IT-CCBC is similar to that of Ir/C in the low-current range, while it is similar to that of Pt/C in the high-current range. During charge, IT-CCBC greatly outperforms Pt/C with much-reduced battery voltage, demonstrating very similar results compared

DOI: 10.1021/am507470f
ACS Appl. Mater. Interfaces 2015, 7, 902–910

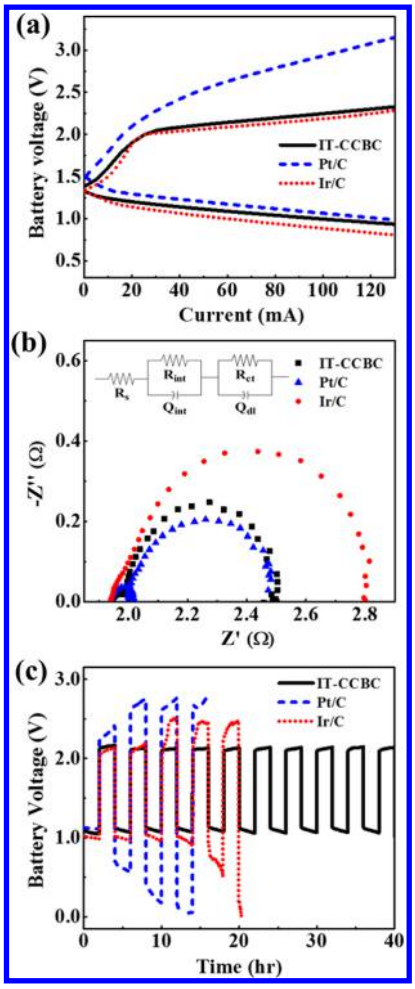

Figure 7. (a) Galvanodynamic charge/discharge profiles. (b) Nyquist plots. (inset) Equivalent circuit. (c) Galvanostatic charge/discharge cycling of IT-CCBC, Pt/C, and Ir/C obtained by utilizing realistic rechargeable zinc−air battery.

to those of Ir/C. The excellent single-cell zinc−air battery performance demonstrated by IT-CCBC here clearly shows its cost competitiveness over precious metal-based commercial catalysts. In addition to the galvanodynamic behavior, EIS is used to further examine the resistances associated with the zinc−air battery operation as shown by the Nyquist plot in Figure 7b with the equivalent circuit. The Nyquist plot consists of two semicircles that are modeled by an equivalent circuit with five elements R_s, Q_{int}, R_{ini}, Q_{dl}, and R_{ct} consistent with previous reports on metal−air batteries.[34,35] R_s and R_{ini} represent electrolyte and contact resistance, and solid−liquid electrolyte interface resistance, respectively. Q_{int} and Q_{dl} are characteristic of the capacitance at the interface of electrode and the electrolyte in the battery, respectively. R_{ct} represents the charge-transfer resistance of the air cathode during the electrochemical reactions, which is directly related to the degree of the catalytic activity of the catalyst. On the basis of the equivalent circuit, the values of the elements are determined and shown in Supporting Information, Table S1, where very comparable charge-transfer resistances of 0.50 and 0.46 ohms are observed with IT-CCBC and Pt/C, respectively, consistent with the galvanodynamic discharge performance. Ir/C demonstrates the highest charge-transfer resistance, which is not favorable for the battery discharge process. The cycle stability of the battery is assessed by conducting the galvanostatic C/D cycling by applying a fixed current of 50 mA with each cycle being 4 h (2 h of discharge followed by 2 h of charge) as shown in Figure 7c. IT-CCBC shows excellent cycle stability with virtually no voltage fading for both discharge and charge profiles even after 40 h of continuous operation. In contrast, the commercial Pt/C and Ir/C catalysts demonstrated limited cycle stability of less than 15 and 20 h of operation, respectively, resulting in significant charge and discharge voltage fading. Additionally, the promising charge/discharge performance and cycle stability obtained by using IT-CCBC is very respectable compared to other rechargeable zinc−air battery performance reported in the literature (Supporting Information, Table S2). Lastly, IT-CCBC, compared to our previously reported core−corona bifunctional catalyst (CCBC), shows significantly improved ORR and OER properties tested in half-cell as well as zinc−air battery performance as summarized in Table 1. The half-cell ORR and OER current densities of IT-CCBC are much superior for both before and after 500 cycles of FDT durability testing, which is indicative of enhanced electrocatalytic activity and electrochemical stability. The zinc−air battery testing shows significantly better charge and discharge battery potentials with IT-CCBC, which leads to greater efficiency. These advancements in electrochemical performance are attributed to the advanced intertwined morphology of NCNT encapsulating $LaNiO_3$ NP cluster, which in turn creates strong interactions between NCNT and $LaNiO_3$ NP for improved charge transfer during the oxygen reactions.

CONCLUSION

In this study, we introduce a bifunctional composite catalyst IT-CCBC highly active and durable toward both oxygen reduction and evolution reactions for rechargeable metal−air battery applications. The catalyst has a unique morphology consisting of size-controlled perovskite $LaNiO_3$ NP encapsulated by highly porous intertwined NCNT network with superior surface area and pore volume. The ORR and OER activities

Table 1. Summary of Half-Cell and Rechargeable Zinc−Air Battery Testing Results of IT-CCBC and Previously Reported CCBC

	half-cell testing				zinc−air battery	
	before FDT		after FDT (500 cycles)		(C/D cycle)	
	J_{ORR},[a] mA cm^{-2}	J_{OER},[a] mA cm^{-2}	J_{ORR},[a] mA cm^{-2}	J_{OER},[a] mA cm^{-2}	$V_{discharge}$,[b] V	V_{charge},[b] V
IT-CCBC	3.27	27.0	2.38	24.9	1.02	2.17
CCBC	2.83	19.7	1.34	15.4	0.94	2.35

[a] J_{ORR} and J_{OER} represent ORR and OER current densities measured at 0.7 V (vs RHE) and 1.95 V (vs RHE), respectively. [b] $V_{discharge}$ and V_{charge} represent the minimum and maximum voltage at 75th cycle during pulse C/D cycle testing using the rechargeable zinc−air battery prototype. The values for CCBC are obtained from the previous report.[15]

DOI: 10.1021/am507470f
ACS Appl. Mater. Interfaces 2015, 7, 902−910

are mainly attributed to NCNT and $LaNiO_3$ NP, respectively; however as a composite, IT-CCBC exhibits excellent synergistic catalytic effect. In fact, the composite outperforms the state-of-art commercial Pt/C catalyst in terms of both ORR and OER activities as well as electrochemical durability. The practicality of the catalyst is further highlighted by excellent charge/discharge performances and cyclability in a realistic rechargeable zinc−air battery utilizing atmospheric air in ambient conditions. These half-cell testing and practical rechargeable zinc−air battery measurements are indicative of excellent synergistic activity and durability of IT-CCBC, which is attributed to small particle sizes of $LaNiO_3$ NP providing enhanced growth sites for prolific growth of intertwined NCNT. This composite with strong interparticle interaction leads to rapid charge transfer and diffusion of reactants during the electrochemical oxygen reactions. This work is a direct demonstration of advancement in bifunctional catalyst development, which utilizes highly engineered composite morphology design to enhance catalytic activity and durability for commercialization of high-performance rechargeable metal−air batteries.

■ ASSOCIATED CONTENT

Supporting Information

SEM and TEM images of NCNT. Thermogravimetric analysis of IT-CCBC. Koutechý−Levich plot and calculation of electron-transfer numbers during ORR. Schematic illustration of single-cell rechargeable zinc−air battery prototype. Values of the equivalent circuit elements from EIS. Performance of rechargeable zinc−-air battery published in the literature. This material is available free of charge via the Internet at http://pubs.acs.org.

■ AUTHOR INFORMATION

Corresponding Author

*E-mail: zhwchen@uwaterloo.ca. Phone: 1-519-888-4567 ext. 38664. Fax: 1-519-746-4979.

Notes

The authors declare no competing financial interest.

■ ACKNOWLEDGMENTS

This research was supported by the Natural Sciences and Engineering Research Council of Canada (NSERC) through grants to Z.C. and the University of Waterloo.

■ REFERENCES

(1) Liang, Y.; Li, Y.; Wang, H.; Dai, H. Strongly Coupled Inorganic/Nanocarbon Hybrid Materials for Advanced Electrocatalysis. *J. Am. Chem. Soc.* **2013**, *135*, 2013−2036.

(2) Hwang, H. J.; Koo, J.; Park, M.; Park, N.; Kwon, Y.; Lee, H. Multilayer Graphynes for Lithium Ion Battery Anode. *J. Phys. Chem. C* **2013**, *117*, 6919−6923.

(3) Park, H. W.; Lee, D. U.; Nazar, L. F.; Chen, Z. Oxygen Reduction Reaction Using MnO2 Nanotubes/Nitrogen-Doped Exfoliated Graphene Hybrid Catalyst for Li-O2 Battery Applications. *J. Electrochem. Soc.* **2013**, *160*, A344−A350.

(4) Bruce, P. G.; Freunberger, S. A.; Hardwick, L. J.; Tarascon, J.-M. Li-O2 and Li-S batteries with high energy storage. *Nat. Mater.* **2012**, *11*, 19−29.

(5) Lee, J. S.; Kim, S. T.; Cao, R.; Choi, N. S.; Liu, M.; Lee, K. T.; Cho, J. Metal-Air Batteries with High Energy Density: Li-Air versus Zn-Air. *Adv. Energy Mater.* **2011**, *1*, 34−50.

(6) Wang, Z.-L.; Xu, D.; Xu, J.-J.; Zhang, X.-B. Oxygen electrocatalysts in metal−air batteries: from aqueous to nonaqueous electrolytes. *Chem. Soc. Rev.* **2014**, *43*, 7746−7786.

(7) Du, G.; Liu, X.; Zong, Y.; Hor, T. S. A.; Yu, A.; Liu, Z. Co3O4 nanoparticle-modified MnO2 nanotube bifunctional oxygen cathode catalysts for rechargeable zinc−air batteries. *Nanoscale* **2013**, *5*, 4657−4661.

(8) Christensen, J.; Albertus, P.; Sanchez-Carrera, R. S.; Lohmann, T.; Kozinsky, B.; Liedtke, R.; Ahmed, J.; Kojic, A. A Critical Review of Li/Air Batteries. *J. Electrochem. Soc.* **2012**, *159*, R1−R30.

(9) Wu, J.; Park, H. W.; Yu, A.; Higgins, D.; Chen, Z. Facile Synthesis and Evaluation of Nanofibrous Iron−Carbon Based Non-Precious Oxygen Reduction Reaction Catalysts for Li−O2 Battery Applications. *J. Phys. Chem. C* **2012**, *116*, 9427−9432.

(10) Park, H. W.; Lee, D. U.; Liu, Y.; Wu, J.; Nazar, L. F.; Chen, Z. Bi-Functional N-Doped CNT/Graphene Composite as Highly Active and Durable Electrocatalyst for Metal Air Battery Applications. *J. Electrochem. Soc.* **2013**, *160*, A2244−A2250.

(11) Yu, T.; Kim, D. Y.; Zhang, H.; Xia, Y. N. Platinum Concave Nanocubes with High-Index Facets and Their Enhanced Activity for Oxygen Reduction Reaction. *Angew. Chem., Int. Ed.* **2011**, *50*, 2773−2777.

(12) Lu, Y. C.; Xu, Z. C.; Gasteiger, H. A.; Chen, S.; Hamad-Schifferli, K.; Shao-Horn, Y. Platinum-Gold Nanoparticles: A Highly Active Bifunctional Electrocatalyst for Rechargeable Lithium-Air Batteries. *J. Am. Chem. Soc.* **2010**, *132*, 12170−12171.

(13) Lim, B.; Jiang, M. J.; Camargo, P. H. C.; Cho, E. C.; Tao, J.; Lu, X. M.; Zhu, Y. M.; Xia, Y. N. Pd-Pt Bimetallic Nanodendrites with High Activity for Oxygen Reduction. *Science* **2009**, *324*, 1302−1305.

(14) Lee, Y.; Suntivich, J.; May, K. J.; Perry, E. E.; Shao-Horn, Y. Synthesis and Activities of Rutile IrO2 and RuO2 Nanoparticles for Oxygen Evolution in Acid and Alkaline Solutions. *J. Phys. Chem. Lett.* **2012**, *3*, 399−404.

(15) Chen, Z.; Yu, A. P.; Higgins, D.; Li, H.; Wang, H. J.; Chen, Z. W. Highly Active and Durable Core-Corona Structured Bifunctional Catalyst for Rechargeable Metal-Air Battery Application. *Nano Lett.* **2012**, *12*, 1946−1952.

(16) Liang, Y. Y.; Li, Y. G.; Wang, H. L.; Zhou, J. G.; Wang, J.; Regier, T.; Dai, H. J. Co3O4 nanocrystals on graphene as a synergistic catalyst for oxygen reduction reaction. *Nat. Mater.* **2011**, *10*, 780−786.

(17) Wang, L.; Zhao, X.; Lu, Y. H.; Xu, M. W.; Zhang, D. W.; Ruoff, R. S.; Stevenson, K. J.; Goodenough, J. B. CoMn2O4 Spinel Nanoparticles Grown on Graphene as Bifunctional Catalyst for Lithium-Air Batteries. *J. Electrochem. Soc.* **2011**, *158*, A1379−A1382.

(18) Liu, Y.; Higgins, D. C.; Wu, J.; Fowler, M.; Chen, Z. Cubic spinel cobalt oxide/multi-walled carbon nanotube composites as an efficient bifunctionalelectrocatalyst for oxygen reaction. *Electrochem. Commun.* **2013**, *34*, 125−129.

(19) Suntivich, J.; May, K. J.; Gasteiger, H. A.; Goodenough, J. B.; Shao-Horn, Y. A Perovskite Oxide Optimized for Oxygen Evolution Catalysis from Molecular Orbital Principles. *Science* **2011**, *334*, 1383−1385.

(20) Yang, W.; Salim, J.; Li, S.; Sun, C.; Chen, L.; Goodenough, J. B.; Kim, Y. Perovskite Sr0.95Ce0.05CoO3-[small delta] loaded with copper nanoparticles as a bifunctional catalyst for lithium-air batteries. *J. Mater. Chem.* **2012**, *22*, 18902−18907.

(21) Suntivich, J.; Gasteiger, H. A.; Yabuuchi, N.; Nakanishi, H.; Goodenough, J. B.; Shao-Horn, Y. Design principles for oxygen-reduction activity on perovskite oxide catalysts for fuel cells and metal−air batteries. *Nat. Chem.* **2011**, *3*, 546−550.

(22) Li, G. G.; Li, C. X.; Xu, Z. H.; Cheng, Z. Y.; Lin, J. Facile synthesis, growth mechanism and luminescence properties of uniform La(OH)(3): Ho3+/Yb3+ and La2O3: Ho3+/Yb3+ nanorods. *CrystEngComm* **2010**, *12*, 4208−4216.

(23) Li, J. X.; Yang, M.; Wei, J. P.; Zhou, Z. Preparation and electrochemical performances of doughnut-like Ni(OH)(2)-Co(OH)(2) composites as pseudocapacitor materials. *Nanoscale* **2012**, *4*, 4498−4503.

DOI: 10.1021/am507470f
ACS Appl. Mater. Interfaces 2015, 7, 902−910

(24) Barde, F.; Palacin, M. R.; Beaudoin, B.; Christian, P. A.; Tarascon, J. M. Cationic substitution in gamma-type nickel (oxi)-hydroxides as a means to prevent self-discharge in Ni/Zn primary batteries. *J. Power Sources* **2006**, *160*, 733−743.
(25) Li, Y. L.; Wang, J. J.; Li, X. F.; Liu, J.; Geng, D. S.; Yang, J. L.; Li, R. Y.; Sun, X. L. Nitrogen-doped carbon nanotubes as cathode for lithium-air batteries. *Electrochem. Commun.* **2011**, *13*, 668−672.
(26) Wei, D.; Liu, Y.; Wang, Y.; Zhang, H.; Huang, L.; Yu, G. Synthesis of N-Doped Graphene by Chemical Vapor Deposition and Its Electrical Properties. *Nano Lett.* **2009**, *9*, 1752−1758.
(27) Ma, G. X.; Zhao, J. H.; Zheng, J. F.; Zhu, Z. P. Synthesis of nitrogen-doped graphene and its catalytic activity for the oxygen reduction reaction in fuel cells. *Carbon* **2012**, *27*, 258−265.
(28) Qu, L. T.; Liu, Y.; Baek, J. B.; Dai, L. M. Nitrogen-Doped Graphene as Efficient Metal-Free Electrocatalyst for Oxygen Reduction in Fuel Cells. *ACS Nano* **2010**, *4*, 1321−1326.
(29) Zhu, S. M.; Chen, Z.; Li, B.; Higgins, D.; Wang, H. J.; Li, H.; Chen, Z. W. Nitrogen-doped carbon nanotubes as air cathode catalysts in zinc−air battery. *Electrochim. Acta* **2011**, *56*, 5080−5084.
(30) Lee, D. U.; Park, H. W.; Higgins, D.; Nazar, L.; Chen, Z. Highly Active Graphene Nanosheets Prepared via Extremely Rapid Heating as Efficient Zinc-Air Battery Electrode Material. *J. Electrochem. Soc.* **2013**, *160*, F910−F915.
(31) Li, H.; Liu, H.; Jong, Z.; Qu, W.; Geng, D.; Sun, X.; Wang, H. Nitrogen-doped carbon nanotubes with high activity for oxygen reduction in alkaline media. *Int. J. Hydrogen Energy* **2011**, *36*, 2258−2265.
(32) Ma, Y.; Sun, L.; Huang, W.; Zhang, L.; Zhao, J.; Fan, Q.; Huang, W. Three-Dimensional Nitrogen-Doped Carbon Nanotubes/Graphene Structure Used as a Metal-Free Electrocatalyst for the Oxygen Reduction Reaction. *J. Phys. Chem. C* **2011**, *115*, 24592−24597.
(33) Kondo, S.; Nakamura, M.; Maki, N.; Hoshi, N. Active Sites for the Oxygen Reduction Reaction on the Low and High Index Planes of Palladium. *J. Phys. Chem. C* **2009**, *113*, 12625−12628.
(34) Zhang, G. Q.; Zhang, X. G.; Li, H. L. Self-assembly preparation of mesoporous hollow nanospheric manganese dioxide and its application in zinc−air battery. *J. Solid State Electrochem.* **2006**, *10*, 995−1001.
(35) Lee, D. U.; Choi, J. Y.; Feng, K.; Park, H. W.; Chen, Z. Advanced Extremely Durable 3D Bifunctional Air Electrodes for Rechargeable Zinc-Air Batteries. *Adv. Energy Mater.* **2013**, DOI: 10.1002/aenm.201301389.

DOI: 10.1021/am507470f
ACS Appl. Mater. Interfaces 2015, 7, 902−910